Quantitative Assessment of Cerebral Blood Flow in Patients with Alzheimer's Disease by SPECT

Peter Bartenstein, Satoshi Minoshima, Christine Hirsch, Katharina Buch, Frode Willoch, Dagmar Mösch, Daniel Schad, Markus Schwaiger and Alexander Kurz

Departments of Nuclear Medicine and Psychiatry, Technical University Munich, Munich, Germany; and Division of Nuclear Medicine, Department of Internal Medicine, The University of Michigan, Ann Arbor, Michigan

This study evaluated an automated analysis of SPECT brain imaging in patients with Alzheimer's disease (AD). **Methods:** Patients [n = 81; mean age, 69.9 ± 10.6 yr (mean ± s.d.)] with a clinical diagnosis of probable AD (NINCDS-Alzheimer's Disease and Related Disorders Association criteria) underwent ^{99m}Tc-ethyl cysteine dimer SPECT imaging. After imaging registration and data extraction using three-dimensional stereotactic surface projections, a pixel-wise comparison of ethyl cysteine dimer uptake was performed using a reference database of 10 cognitive intact controls of comparable age. **Results:** When individual cases were compared to the normal database, temporo-parietal regional cerebral blood flow (rCBF) abnormalities across different levels of dementia severity were clearly depicted on pixel-wise Z-score images. The rCBF reduction in cortical association areas showed a significant correlation with an overall level of cognitive decline, as assessed by the Mini Mental State Examination and by the cognitive section of the Cambridge Mental Disorders of the Elderly Examination. In addition, there were significant region-specific correlations between left temporo perfusion deficit and language performance and between right parietal rCBF reduction and praxis. **Conclusion:** These results indicate that this observer-independent analysis of SPECT data enables objective and semiquantitative assessment of the magnitude and extent of cortical perfusion abnormalities in patients with AD.

Key Words: SPECT; computer-assisted image processing; Alzheimer's disease; cognitive dysfunction

J Nucl Med 1997; 38:1095–1101

In Alzheimer's disease (AD), the measurement of regional cerebral blood flow (rCBF) using SPECT reveals a decreased cortical perfusion that is typically predominant in the temporal and parietal cortices (*1,2*). This pattern matches that of the metabolic abnormalities that can be revealed in AD patients using a more sensitive method of positron emission CT (*2,3*). Such region-specific rCBF reduction is often associated with lateralized cognitive functions such as language and praxis (*4*). In vivo rCBF measurement by SPECT, which reflects cortical topography of pathophysiologic changes in AD seen at neuropathological examination (*5*), is a valuable aid in the early recognition of AD and in its differentiation from other dementing disorders. Both are important diagnostic tasks, as most effective interventions currently available are specific to AD (*6*) and because AD must be distinguished from potentially treatable causes of dementia such as depression or normal pressure hydrocephalus.

Particularly in patients with mild dementia, the ability to recognize rCBF patterns of AD by visual interpretation is highly dependent on the quality of SPECT images and levels of experience of observers (*7,8*). To reduce interobserver variability in the evaluation of brain SPECT studies and to allow more accurate assessment of the extent and severity of rCBF abnormalities, observer-independent methods for the analysis of SPECT data that provide an objective measurement of perfusion abnormalities are desired.

This study focuses on the first application of a fully automated, user-independent analytical method (*9*) for SPECT imaging. Because SPECT is less costly than PET and more widely available, the transfer of advanced analytical methods developed for PET to SPECT will improve the analysis of SPECT data, not only for scientific purposes but also for clinical routine use. In addition to evaluating this analytic approach in a large population of AD patients, we examined whether this new technique is capable of demonstrating relationships between cognitive abnormalities, as assessed in neuropsychological testing, and rCBF abnormalities in regions attributed to these cognitive domains.

MATERIALS AND METHODS

Subjects

Cognitive functions and rCBF impairment were studied in 81 patients (52 women, 29 men) who were diagnosed as having probable AD according to NINCDS Alzheimer's Disease and Related Disorders Association criteria, based on thorough clinical evaluation (*10*). The mean age at the time of examination was 70 ± 11 yr (mean ± s.d.), and the estimated mean age of onset was 67 ± 10 yr. The mean score on the Mini Mental State Examination (MMSE) (*11*) was 20.1 ± 4.6 points (mean ± s.d.) at the time of the SPECT scan. This indicates that the patient population included subjects with an early onset and with a mild degree of symptoms.

In addition to the clinical diagnosis of AD, the inclusion criteria consisted of being right-handed and having an interval between cognitive testing and the SPECT study of less than 3 mo. Very mild cases were only included in the analysis when they fulfilled the clinical criteria for probable AD in a subsequent clinical follow up. According to the terziles of the MMSE distribution, the patients were allocated to three levels of dementia severity: very mild (>23 points, n = 29; group 1), mild (22–18 points, n = 25; group 2) and moderate to severe (<18 points, n = 27; group 3).

In addition, rCBF SPECT was performed in 10 cognitively intact right-handed normal control subjects (5 women, 5 men) of similar age [64 ± 7.5 yr (mean ± s.d.)]. Permission to obtain these data was given by the Ethics Committee of the Technische Universität München and by the radiation protection authorities.

Cognitive Assessment

Cognitive functions were evaluated using an appropriate section (CAMCOG) of the Cambridge Mental Disorders of the Elderly Examination (*12*). The section covers eight cognitive domains (orientation, language, memory, attention, praxis, calculation, abstract thinking and perception) and has a maximum score of 107. To examine the relationship between rCBF measures and lateral-

Received May 15, 1996; revision accepted Nov. 6, 1996.

For correspondence or reprints contact: Peter Bartenstein, MD, Nuklearmedizinische Klinik und Poliklinik, der Technischen Universität München, Klinikum rechts der Isar, Ismaninger Strasse 22, 81675 München, Germany.

ized cognitive functions, we selected the language and praxis CAMCOG subscores. The praxis score includes visuospatial skills, such as figure copying.

Imaging Technique

rCBF was measured with a high-resolution SPECT using ^{99m}Tc ethyl cysteine dimer (ECD) (Neurolite®). All SPECT studies were performed with a triple-head rotating gamma camera (Siemens Multispect 3) under a standard resting condition (eyes open in dimmed ambient light). The image acquisition started 30 min after intravenous administration of 750 MBq ^{99m}Tc ECD and lasted over 30 min (40 projection images per detector head, 45 sec per image, 360°). The distance of the collimators from the center of rotation was kept constant at 12.8 cm. A low-energy, high-resolution collimator and a 128 × 128 acquisition matrix were used for data acquisition. Images were reconstructed with a Butterworth filter (cutoff frequency 0.4/order 7) resulting in a reconstructed resolution (FWHM) of approximately 13 mm at the center of rotation. A reconstructed pixel size was 3.56 mm. Attenuation was corrected according to Chang's technique using an absorption coefficient of 0.16 cm^{-1} (*13*).

Image Analysis

To measure the relative decrease of ECD uptake, a semiquantitative analytic approach that was originally developed for PET images (*9,14–17*) was adapted for SPECT images and described in the following sections. Image analysis was performed on a SPARC 2 workstation (Sun Microsystems Inc., Mountain View, CA).

Determination of the Reference Region

In the first step, we compared the internal reference regions suitable for data normalization. The brain images of the 10 controls were standardized anatomically to the stereotactic coordinate system proposed by Talairach et al. (*18*), and three-dimensional stereotactic surface projections (3D-SSPs) were generated (see below) (*9*). These standardized datasets were normalized to the global mean, thalamus, pons and cerebellum. For thalamic normalization, the average value of 20 pixels with the highest ECD uptake within the thalamus was determined separately for each hemisphere. For cerebellar normalization, the average value of 618 pixels encompassing the lateral cerebellum was determined for each hemisphere. Because functional deactivation induced by the more severely affected hemisphere in AD could reduce rCBF in the ipsilateral thalamus and contralateral cerebellum (*19*), the side containing a higher average value was selected for normalization. For pontine normalization, the average value of 150 pixels covering the entire pons was chosen. Each surface pixel was then divided by a reference value. From these normalized datasets, mean and s.d. images were generated for each reference value. Coefficients of variation (s.d./mean) were assessed for each hemisphere separately by a single region of interest encompassing all cortical pixels. Coefficients of variation for each reference region were compared to that derived from normalization to a global mean activity.

Image Processing of Individual SPECT Data

The thalamus was chosen as a reference region for the subsequent analysis of the patient data. Three steps of completely automated analysis will be described in the following sections.

Stereotactic anatomic standardization. In the initial step, a rotational correction and a centering in three dimensions of the SPECT dataset were performed (*14*), followed by a realignment to the AC–PC line. The AC–PC line was defined in the midsagittal plane by four anatomic landmarks (frontal pole, inferior end of the anterior corpus callosum, inferior point of thalamus and occipital pole) (*15*).

To adjust the individual brain to the proportional grid system proposed by Talairach et al. (*18*), the brain image was resized to the standard dimensions according to calculated linear scale factors. After linear correction for an individual brain size, regional anatomic differences between the individual and the atlas brain were minimized by an automated nonlinear warping technique with special regard to regional mismatches of the cortical ribbon and subcortical structures (*16*). The warping was based on sets of stretching centers, predominantly in the white matter, and on more than 250 predefined gray matter landmarks for each hemisphere. These centers and landmarks were derived based on directions of major neuronal fiber pathways. Individual's surface landmarks were searched iteratively between predefined centers and surface landmarks using a profile curve analysis. Detected individual's landmarks were then warped to predefined landmarks, resulting in a standardized image set with a uniform voxel size of 2.25 mm.

Data extraction using 3D-SSPs. Gray matter activity in the brain was extracted using 3D-SSPs (*9*). In this approach, the outer brain contour covering the entire lateral and medial hemispheres was predefined on a standard atlas. For each predefined contour pixel, a peak cortical pixel was searched in a standardized individual's image set on a predefined line perpendicular to the standard atlas contour with a search depth of 6 pixels. The search depth was equal to 13.5 mm, which approximately covers gray matter peak activity on SPECT image sets. The peak cortical pixel value was assigned to a corresponding surface pixel (surface projection), and the search was repeated for all predefined contour pixels (*9*). The extracted 3D-SSP data could be viewed from superior, inferior, right, left, anterior, posterior and two medial aspects of the brain (both lateral views and a superior view are displayed in Fig. 2).

Comparison of the individual stereotactically normalized data with the dataset of normal control subjects. Before a normal database comparison, thalamic normalization was performed as described previously. To quantify perfusion deficits, normalized brain activity of each patient was compared with the reference normal database consisted of 10 normal control subjects by means of a Z-score. A Z-score is computed on a pixel-by-pixel basis on the 3D-SSP format according to the following formula (*9*):

$$\text{Z-score}_{(x,y,z)} = (N_{mean(x,y,z)} - AD_{(x,y,z)})/N_{sd(x,y,z)},$$

where $N_{mean(x,y,z)}$ and $N_{sd(x,y,z)}$ represent the mean and s.d. in the normal control subjects at stereotactic coordinates (x,y,z). $AD_{(x,y,z)}$ represents normalized rCBF of an individual patient at the same pixel coordinates. A positive Z-score represents a reduced rCBF in the patient relative to the control mean. Surface projection views of the Z-score were created in the same manner as that for individual rCBF surface projections (Fig. 2).

Because the entire procedure is fully automated, there was no interobserver variability in this analysis. Ten patients who were processed independently by two different investigators yielded identical results. Computational time was less than 60 min per case on the SPARC 2. During this time, no interference by the user was necessary. At the end of the entire procedure, visual quality assurance of the landmark detection was performed. In five cases, intense scalp or other soft tissue uptake (i.e., temporal muscle) interfered with the procedure of anatomic standardization. In such cases, manual removal of the scalp activity was required.

Statistical Analysis

A predefined set of regions of interest (ROIs) covering the frontal, temporal and parietal lobes of each hemisphere and an additional region combining the temporal and parietal areas were positioned on Z-score images sparing a region near the central sulcus. Mean and maximum Z-scores of each ROI were used for

TABLE 1
Patient I.D.: Cognitive profile

CAMCOG subcomponents	Score	% of maximum
Language	13	43
Memory	4	15
Praxis	3	25
Perception	2	18

subsequent analyses. The frontal, temporal and parietal lobe ROIs covered 2090, 1539 and 1595 surface pixels, respectively.

To assess a sensitivity of the proposed analytical method in the detection of rCBF abnormalities in regions affected in AD, the unilateral and bilateral occurrence of three adjacent pixels with a Z-score above 2 in the temporo-parietal region of the three groups with very mild (group 1), mild (group 2) and moderate to severe dementia (group 3) was examined. To address a specificity of the proposed method, the occurrence of three adjacent pixels with a Z-score above 2 in the temporo-parietal regions was examined also in each normal subject in comparison to a reference normal database consisting of other nine normal subjects.

To measure global rCBF deviation in the association cortex, a mean Z-score of the left and right frontal, temporal and parietal ROIs was computed. The correlation between this average rCBF deviation and overall cognitive impairment was examined by Spearman's correlation. Differences in the average rCBF deviation among the three patient groups were examined also using the Kruskal–Wallis test. Two-group differences were analyzed with the Mann–Whitney test. To explore correlations between regional brain perfusion deficits and selected cognitive functions, multiple regression models were applied which included age, gender, years of formal education and professional training, duration of illness and regional perfusion parameters as independent variables and respective cognitive functions as dependent variables.

Case Example

A typical patient may clearly illustrate the method applied. A 73-yr-old woman (Patient I.D.), a former psychologist, presented with AD of moderate severity (MMSE, 17 points; CAMCOG, 33 points). The pattern of cognitive functions and rCBF abnormalities are summarized in Tables 1 and 2. Figure 1 shows transverse slices of patient's original brain SPECT images and corresponding images after stereotactic anatomic normalization. 3D-SSP images of rCBF and Z-score in comparison with the normal database are demonstrated with different views of the brain in Figure 2. The right and left lateral views in the upper row show temporo-parietal rCBF decrease bilaterally. In this patient, the temporo-parietal hypoperfusion is more pronounced on the right side compared to that on the left side. This corresponds very well to severe impairment in performance of praxis in the CAMCOG test, which can be attributed to the right hemisphere. Relatively mild language impairment corresponds to the mild reduction of rCBF in the left hemisphere. Perfusion in the frontal lobe seems to be relatively preserved, consistent with no affective abnormality in this patient.

TABLE 2
Patient I.D.: Individual rCBF Reduction Compared to the Normal Database

	rCBF reduction mean in Z-scores (maximum)
Right temporal	3.5 (12.6)
Right parietal	4.5 (11.0)
Right frontal	0.8 (4.0)
Left temporal	1.0 (4.2)
Left parietal	1.9 (6.4)
Left frontal	0.5 (3.8)
Global mean	2.0

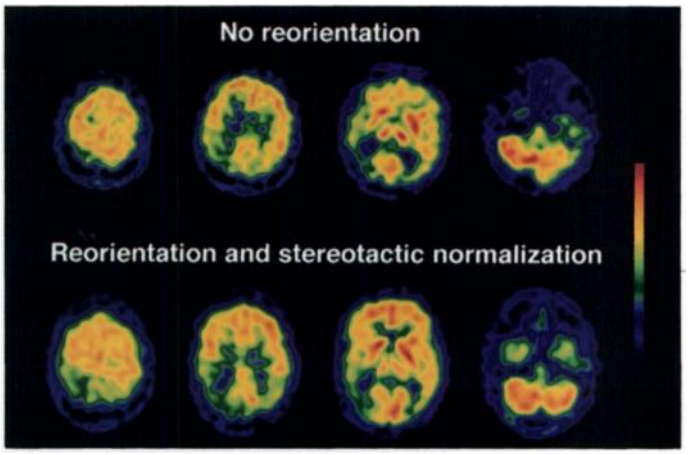

FIGURE 1. SPECT brain images of patient I. D. showing original transverse slices before alignment to the AC–PC line (upper) and approximately corresponding slices after automatic realignment and stereotactic normalization (bottom).

RESULTS

Comparison of Reference Regions for Normalization in Normal Subjects

Results of comparison among mean cortical coefficients of variation derived from different references for pixel normalization were as follows. Normalization to the global mean resulted in mean cortical coefficients of variation of 6.6% in the right hemisphere and 7.5% in the left hemisphere (7.1% for both hemispheres). Thalamic normalization resulted in a slightly higher mean cortical coefficients of variation. They were 8.9% for the right side, 9.0% for the left side and 9.0% for both hemispheres. Cerebellar normalization induced an increase in the variability of the cortical surface pixels in the normal database (9.5%, right side; 10.6%, left side; 10.0%, both hemispheres). Normalization to the pons revealed even larger coefficients of variation: 10.0% for the right side, 11.0% for the left side and 10.7% for both hemispheres. Figure 3 provides visual assessment of coefficients of variation calculated using different reference regions for pixel normalization.

Detection of Temporo-Parietal Perfusion Abnormalities in AD Patients

In the 81 patients with probable AD, the proposed analytic approach showed a decrease in temporo-parietal rCBF (deter-

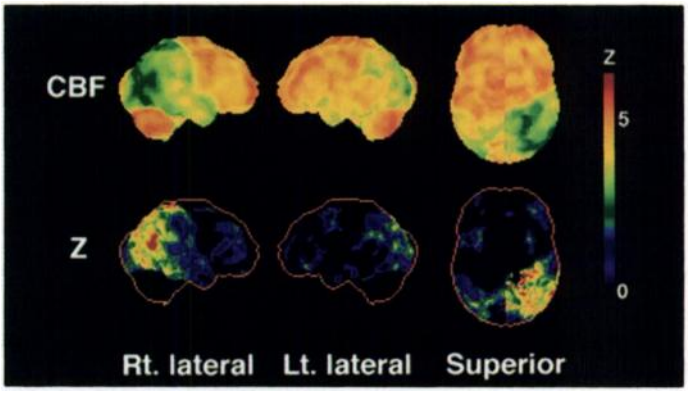

FIGURE 2. 3D-SSPs of CBF SPECT data of patient I. D. (upper) showing right lateral, left lateral and superior views. Corresponding views (bottom) of statistical Z-score images demonstrating areas of rCBF reduction in this patient in comparison to the normal database. The color of the outer contour corresponds to a Z-score of 5.

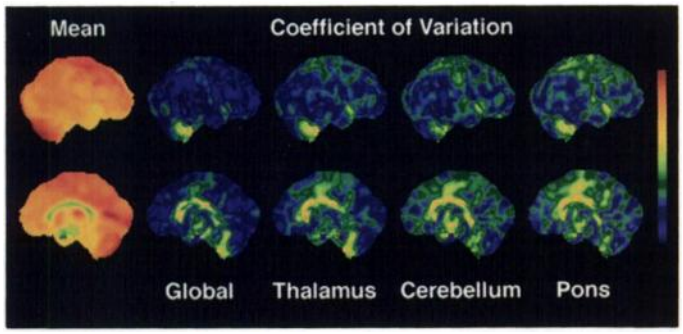

FIGURE 3. Right lateral view (upper) and right medial view (bottom) of 3D-SSPs of the normal database (n = 10). From left to right: mean image and coefficient of variation images for normalization to the global mean, thalamus, cerebellum and pons. For illustrative purposes, different color scales were used for the mean image (maximum, 1.25) and for the coefficient of variation images (maximum, 0.3).

mined by three adjacent pixels with a Z-score above 2) in at least one hemisphere in 74 patients (91%) and a bilateral decrease in 62 patients (77%). Across three levels of dementia severities, there was an increased incidence of temporo-parietal perfusion abnormalities with the severity of dementia. In very mildly demented patients (group 1), 24 of 29 patients (83%) had abnormalities in temporo-parietal perfusion in at least one hemisphere. In groups 2 and 3, the incidence increased to 23 of 25 patients (92%) and 27 of 27 patients (100%), respectively. For a bilateral decrease, respective numbers were 17 of 29 (59%) in group 1, 19 of 25 (76%) in group 2 and 26 of 27 (96%) in group 3 (Fig. 4). The analysis of 10 normal subjects revealed bilateral occurrence of three adjacent pixels with a Z-score above 2 in the temporo-parietal region in one case and unilateral occurrence in two cases.

Cognitive Testing and Correlation with rCBF Abnormalities in AD Patients

There was a significant effect of sex on the MMSE and the CAMCOG total score in this particular patient population. Women showed a poorer performance (MMSE, 19.2 ± 4.7 points; CAMCOG, 60.9 ± 15.6 points) than men (MMSE, 21.8 ± 4.0; CAMCOG, 69.5 ± 13.3) ($p = 0.02$ for both sexes). Age was associated with perceptual ability. Mean CAMCOG perception scores were lower in patients at an age above the median of 73 yr (6.0 ± 2.0) than in younger individuals (7.3 ± 2.2; $p = 0.04$).

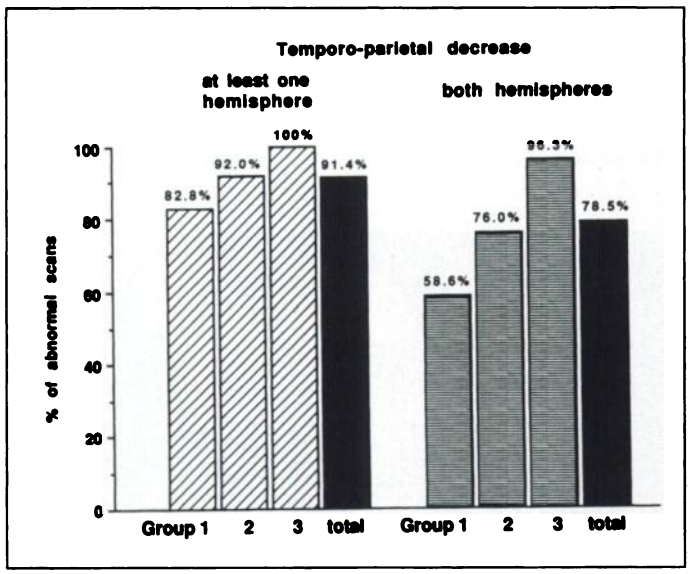

FIGURE 4. Decrease in rCBF in the temporo-parietal region assessed by the appearance of three adjacent pixels above a Z-score of 2 appearing at least in one hemisphere and in both hemispheres. The percentage of patients showing these abnormalities are displayed for the terziles that were very mildly demented (group 1, n = 29), mildly demented (group 2, n = 25) and moderately to severely demented (group 3, n = 27) and for the whole population (n = 81).

TABLE 3
Association Between Relative ECD Uptake and Cognitive Impairment (Average Z-Scores, Multiple Linear Regression)

	Language		Praxis	
Variable	Beta	Significance	Beta	Significance
Deviation of left temporal rCBF	−0.50	**<0.01**	0.19	0.29
Deviation of right temporal rCBF	0.05	0.74	0.03	0.83
Deviation of left parietal rCBF	0.08	0.68	−0.23	0.21
Deviation of right parietal rCBF	−0.17	0.30	−0.41	**<0.01**
Deviation of left frontal rCBF	−0.30	0.03	−0.10	0.47
Deviation of right frontal rCBF	0.27	0.06	0.13	0.35
Age	−0.06	0.63	0.12	0.24
Duration of illness	−0.20	0.05	−0.24	0.02
Years of schooling	0.06	0.55	0.20	0.06
Years of professional training	0.18	0.13	−0.01	0.92
Sex	−0.11	0.33	−0.13	0.29
Multiple R	0.69	**<0.01**	0.66	**<0.01**

The average rCBF reduction in all association cortices of 81 AD patients was 1.38 ± 0.68 (Z-score). Although rCBF asymmetry was evident in individual cases, there was no statistically significant difference ($p > 0.9$, paired Student's t-test) in mean rCBF decrease or maximum Z-score between left and right hemispheres. The average rCBF reduction was correlated significantly with the level of cognitive functioning as assessed with MMSE ($r = -0.44$, $p < 0.0001$) and with CAMCOG ($r = -0.47$, $p < 0.0001$). The correlation was negative because rCBF reduction was expressed as a positive Z-score.

The reduction of averaged rCBF in the cortex was significantly different across the three levels of dementia severity ($p < 0.01$). The mean Z-score was 1.06 ± 0.70 in patients with very mild dementia (group 1), 1.27 ± 0.51 in patients with mild dementia (group 2) and 1.81 ± 0.57 in patients with moderate to severe dementia (group 3).

Multiple linear regression analysis revealed that language performance was correlated with the amount of reduction in relative temporal rCBF on the dominant side. There was an additional loose correlation of left frontal rCBF impairment with language performance (Table 3). In contrast, praxis was significantly associated only with parietal rCBF decrease on the nondominant side. Age had no influence on either cognitive domain, whereas the duration of illness was loosely correlated with both domains. When correcting for gender, duration of formal education and professional training were not significantly correlated with language performance or praxis. With the exception of correlation between praxis and right parietal decrease, higher correlation coefficients were obtained with averaged Z-scores as compared to maximum Z-scores (Table 4). When using maximum Z-scores, the pattern of the correlation remained the same, but the correlation of language performance with rCBF decrease in the left frontal and temporal lobes was no longer significant. For praxis as a dependent variable, there was still an exclusive correlation to right parietal rCBF decrease. Figure 5 illustrates the relationship between language performance and temporal rCBF reduction comparing both sides (Spearman's correlation, no correction for age, gender, duration of illness and education).

TABLE 4
Association between Relative ECD Uptake and Cognitive Impairment (maximum Z-Scores, Multiple Linear Regression)

Variable	Language		Praxis	
	Beta	Significance	Beta	Significance
Deviation of left temporal rCBF	−0.32	0.11	0.01	0.99
Deviation of right temporal rCBF	0.04	0.81	0.17	0.37
Deviation of left parietal rCBF	−0.19	0.29	−0.04	0.83
Deviation of right parietal rCBF	−0.07	0.68	−0.58	**<0.01**
Deviation of left frontal rCBF	−0.23	0.07	−0.04	0.76
Deviation of right frontal rCBF	−0.15	0.28	0.06	0.64
Age	−0.04	0.73	0.13	0.26
Duration of illness	−0.22	0.04	−0.24	0.03
Years of schooling	0.09	0.44	0.14	0.20
Years of professional training	0.26	0.04	0.01	0.91
Sex	−0.04	0.73	−0.14	0.25
Multiple R	0.66	**<0.01**	0.65	**<0.01**

DISCUSSION

In this study, a fully automated, observer-independent analytic approach (*9*) was applied for the first time for semiquantitative analysis of SPECT images. Patterns of rCBF reduction was evaluated in a large, predominantly mildly affected population of patients with probable AD. The incidence of temporoparietal perfusion abnormalities increased with the severity of dementia and reached 100% for a unilateral abnormality in the moderately to severely affected patients. In addition, the extent of rCBF reduction correlated with the severity of disease. Significant correlations between language impairment and left temporal rCBF reduction and between impairment of visuospatial skills and right hemispheric rCBF reduction were demonstrated. These results are consistent with previous knowledge of rCBF abnormalities in AD and support the quantitative accuracy of the proposed method in the evaluation of AD patients.

There are several methods previously proposed to identify cortical rCBF abnormalities on SPECT images in AD patients. Image analysis based on transaxial slices by Johnson et al. (*20*), which uses clusters of macrovoxels for a discriminant analysis, the discriminant function analysis suggested by O'Mahony et al. (*21*) and the principal component analysis suggested by Houston et al. (*22*) all showed a good discriminative power between AD patients and normal control subjects. Similar results were reported using artificial neural networks (*23*). These approaches, however, have certain limitations for their use in a routine clinical setting. Interactive portions of the analyses may require a person dedicated to image processing. Parametric images that visualize the pattern of rCBF abnormality in a way that can be easily communicated to the referring clinician may not be readily available from those approaches. Furthermore, it seems difficult to assess abnormal rCBF patterns in different scans or patients in a consistent way, e.g., to assess progression of the disease or regional improvement of rCBF after treatment. This can be done easily by the proposed method. Because images sets are stereotactically normalized and processed, predefined ROIs encompassing certain cortical areas of interest can be used for all patients and placed on their rCBF images or parametric Z-score images. This allows the assessment of rCBF impairment using multiple parameters, such as the mean or maximum Z-score or the number of pixels with a Z-score above a given threshold.

The approach proposed by Lamoureux et al. (*24*), a quantitative uptake map in a circumferential display, allows a preview of the whole cortical perfusion, but it is hampered by the lack of readily recognizable anatomic structures and the inability to perceive the spatial relationship between lesions. Hooper et al. (*25*) described a method using predefined three-dimensional ROIs. This method allows an easy semiquantitative assessment of perfusion abnormalities but gives no direct visual impression of the pattern of rCBF abnormalities. This analysis is inflexible because it is restricted to 14 predefined regions, and there is a subjective component in the manual definition of the angle of the orbito-meatal plane and fitting of a ROI model.

The proposed analytic approach generates images that have some common appearance to a three-dimensional display method proposed by Hashikawa et al. (*26*), but there are some fundamental differences. Their method uses a similar approach searching pixels with peak cortical activity, but their search directions are fixed from the center of the brain. This approach, therefore, cannot guarantee the anatomic accuracy in resultant projected surface values. In addition, structures that are not perpendicular to a search line from the center of the brain cannot be assessed, e.g., the medial aspect of the brain. Furthermore, it does not enable stereotactic normalization of image data, which is essential for a pixel-wise interindividual comparison. Consequently, observer-independent pixel-by-pixel comparison to a normal reference database using Z-scores, which holds a great diagnostic and analytical power to assess rCBF abnormalities, is not possible by their method.

The substitution of pixels with the maximal value to the corresponding cortical surface used in the present method potentially minimizes partial volume effects due to cortical atrophy. This approach reduces the influence of white matter activity and provides more robust measurement of gray matter activity. In addition, atrophy correction can be incorporated in the proposed method if necessary. However, because the implementation of atrophy correction would rather decrease than increase the sensitivity to detect regional abnormalities and because atrophy itself holds some diagnostic information, it may not be necessary for routine clinical applications (*7*).

As illustrated in the case example, 3D-SSP images allow a simple recognition of rCBF patterns typical for AD, an approach that is likely to increase the diagnostic accuracy of

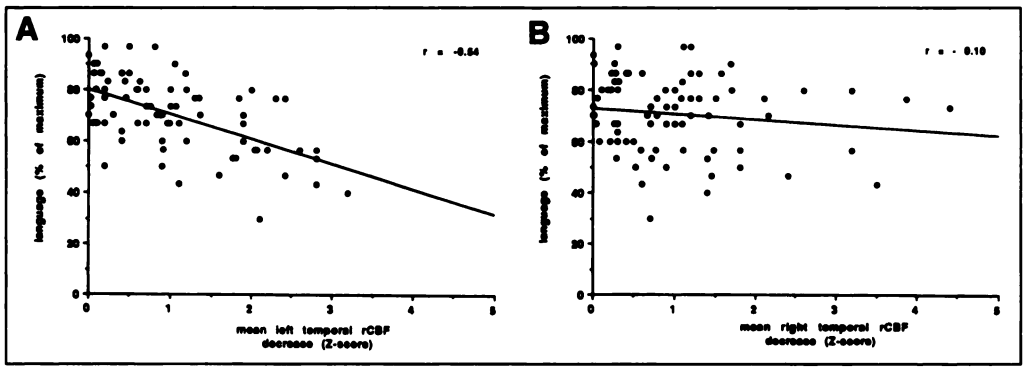

FIGURE 5. (a) Relationship between language performance (% of maximum achievable score) and mean left temporal rCBF reduction compared to the normal database (Z-scores). (b) Relationship between language performance (% of maximum achievable score) and mean right temporal rCBF reduction compared to the normal database (Z-scores).

functional brain imaging (*27,28*). This was tested systematically using PET images (*27*), but not in this SPECT study. However, it was evident from our experience using 3D-SSP images in a large series of over 200 demented patients that patterns of abnormal rCBF were more easily recognizable as compared to conventional slice display. This was especially true when the reader was not experienced and when the abnormalities were not pronounced. Stereotactic normalization in the proposed approach also allows, in contrast to the method proposed by Hashikawa et al. (*26*), consistent localization of rCBF abnormalities in the standard Talairach coordinate system.

The normal database consisted of 10 cognitively intact subjects who were of comparable age but not matched for gender or education. This raises a concern that patients perfusion deficits might have been biased by such uncontrolled factors when they were compared to the normal reference database (*29*). The interindividual variability of relative cortical ECD uptake within the normal dataset, however, seemed to be much greater than the presumed effect of age or gender on cortical perfusion. The effect of the small difference in mean age or education between patients and normal control subjects therefore is not likely affecting the accuracy of the analysis substantially (*29*). In addition, the minor differences in age, gender, and education between patients and controls are not expected to have a systematic effect on the association between rCBF and cognitive function in this study, especially because there was a wide range in age and education within the patients. Certainly, increasing the number of normal subjects and a careful control of subjects' factors will enhance the discriminative power of the analysis.

As expected, the normalization of the cortical activity to the global mean yielded the lowest coefficient of variation but is not suitable for a disease like AD, in which large cortical areas may be affected. The thalamus appeared to be the most robust reference region for SPECT imaging and was, therefore, preferred to other reference regions in this study. The thalamus has a distinct shape and stable perfusion and is located just above the intercommissural line, ensuring reliable and accurate localization. Furthermore, its size is well above the resolution of a modern SPECT system. Although thalamic involvement in AD has been reported, the subcortex is relatively preserved in AD patients (*30*). The suitability of a thalamic reference in AD is supported by O'Brien et al. (*31*), who did not find a significantly reduced rCBF in the thalamus in 35 AD patients, including 21 moderate and severe cases. In some cases of AD, like in stroke, a reduction of rCBF in the thalamus due to functional deactivation from ipsilateral hemispheric abnormalities is imaginable (*19,32*). To circumvent this problem, only the higher value from either hemisphere is used for normalization (*9*).

The cerebellum, which is spared in most cases of AD, would be the ideal reference region and is indeed used by many groups in PET and SPECT imaging (*31,33,34*). However, using the cerebellum as a reference region resulted in a greater variability of relative cortical tracer uptake in the normal database as compared to the thalamus. The cause of the comparatively high variability of relative cerebellar uptake in our normal database is not entirely clear. Partial volume problems are less likely to be responsible in this large structure. The variability of relative cerebellar uptake is perhaps due to the attenuation correction used, which has been shown to introduce more uncertainty in the cerebellum as compared to other reference structures (*35*). The pons, which was used in PET studies as a reliable reference region (*36*), seemed to be affected by the same reason on SPECT images. Basal ganglia have also been used by some authors as a reference region in AD (*34*). When the proposed automated method for SPECT was applied, however, the definition of basal ganglia, particularly concerning separation of the striatum from the adjacent insular cortex or globus pallidus, was so far not reliably possible, and the suitability of this structure as a reference region was not further tested.

The incidence of bilateral temporo-parietal perfusion abnormalities, as the most stereotypical pattern of AD, increased with the severity of disease. In the mildly demented group, the sensitivity in the detection of such abnormalities using the proposed observer-independent approach was comparable to previous results of visual reading of SPECT images by experienced readers (*1,2,7*) and discriminant analysis or principal component analysis (*20–22*). Statements about the specificity for the detection of AD with the proposed method cannot be made in our study because all patients had the diagnosis of probable AD according to the clinical criteria. Although patients that probably suffered from other forms of dementia were involved in our current ongoing research as well, they were not included in this study to determine specificity because so far only very few cases had histopathological diagnosis. We used 2 s.d. (98% probability) as a discriminant threshold, which is commonly used to discriminate abnormalities. Based on the decision strictly made by the above discriminant threshold alone, one of the subjects of the normal database would be classified as having bilateral temporoparietal perfusion abnormalities and therefore defined as abnormal. This subject had unusually wide intraparietal sulci, apparent by visual inspection of the transverse slices and the surface projections, and would have clearly not been suspicious for AD. Therefore, the combination of visual inspection of 3D-SSP images and the use of a quantitative threshold is important when interpreting SPECT data.

Regional CBF abnormalities detected in the AD patients were consistent with clinical testing results. The averaged reduction of ^{99m}Tc ECD uptake was significantly correlated with the overall cognitive impairment. There was a region-specific association between the left temporal reduction and language impairment and between right parietal reduction and praxis. These findings indicate that the proposed analytic approach reliably identified well-known correlations of the nondominant hemisphere with abnormal visuospatial skills and of the dominant hemisphere with language dysfunction, which were established previously by PET investigations (*37*). A more detailed regional correlation was not conducted in the current study because we intended to use common large regions covering areas associated with various cognitive functions. Although smaller regions, e.g., Wernicke's area, could be used for certain specific comparisons, the decision was made to use the same large six regions, each covering an entire lobe, for all analyses of correlation to avoid biases due to size difference and selection of smaller regions and to allow consistent comparisons across correlational analyses. Identification of subgroups of patients, e.g., early- versus late-onset diseases (*38*) would reduce the variability of measurement and may allow for better correlational analysis.

CONCLUSION

The present study suggests that the proposed analytic approach, 3D-SSP SPECT, provides a reliable and objective evaluation of the severity, extent and localization of cortical perfusion abnormalities in patients with AD. This approach allows observer-independent assessment of patterns and severities of rCBF abnormalities using SPECT in AD patients and is applicable to other neurological disorders.

ACKNOWLEDGMENTS

This study is in part supported by grant DE-FG02-87-ER60561 from the U.S. Department of Energy. We thank Mrs. Ursula Ahrens, Monika Krapf, Evi Stadler and Mr. Gernot Leitner for their technical assistance and Mrs. Jodi Neverve for careful review of the manuscript. We also thank Dipl.-Math. Raymonde Busch, Department of Medical Statistics and Epidemiology, Technische Universität München, for her advice and support in the statistical analysis; Edward P. Ficaro, PhD, the Division of Nuclear Medicine, University of Michigan, for his support in processing of the SPECT data; and David E. Kuhl, MD, Division of Nuclear Medicine, University of Michigan, for supporting this collaborative work.

Presented in part at the 23rd Symposium of the European Association of Geriatric Psychiatry, Lund, Sweden, Oct. 6–7, 1995.

REFERENCES

1. Jobst KA, Hindley NJ, King E, Smith AD. The diagnosis of Alzheimer's disease: a question of image? *J Clin Psychiatry* 1994;55(suppl):22–31.
2. Messa C, Perani D, Lucignani G, et al. High-resolution technetium-99-m-HMPAO SPECT in patients with probable Alzheimer's disease: comparison with fluorine-18-FDG-PET. *J Nucl Med* 1994;35:210–216.
3. Heiss WD, Szelies B, Kessler J, Herholz K. Abnormalities of energy metabolism in Alzheimer's disease studied with PET. *Ann NY Acad Sci* 1991;640:65–71.
4. Osimani A, Ichise M, Chung DG, Pogue JM, Freedman M. SPECT for differential diagnosis of dementia and correlation of rCBF with cognitive impairment. *Can J Neurol Sci* 1994;21:104–111.
5. Braak H, Braak E. Neuropathological staging of Alzheimer-related changes. *Acta Neuropathol* 1991;82:239–259.
6. Knapp MJ, Knopman DS, Solomon PR, Pendlebury WW, Davis CS, Gracon SI. A 30-week randomized controlled trial of high-dose tacrine in patients with Alzheimer's disease. *J Am Med Assoc* 1994;271:985–991.
7. Holman BL, Devous MD Sr. Functional brain SPECT: the emergence of a powerful clinical method. *J Nucl Med* 1992;33:1888–1904.
8. Waldemar G, Walowitch RC, et al. Tc-99m bicisate (Neurolite) SPECT brain imaging and cognitive impairment in dementia of the Alzheimer type: a blinded read of image sets from a multicenter SPECT trial. *J Cereb Blood Flow Metab* 1994;14(suppl 1):S99–S105.
9. Minoshima S, Frey KA, Koeppe RA, Foster NL, Kuhl DE. A diagnostic approach in Alzheimer's disease using three-dimensional stereotactic surface projections of fluorine-18-FDG PET. *J Nucl Med* 1995;36:1238–1248.
10. McKhann G, Drachman D, Folstein M, Katzman R, Price D, Stadlan EM. Clinical diagnosis of Alzheimers's disease: report of the NINCDS-ADRDA Work Group under the auspices of Department of Health and Human Services Task Force on Alzheimer's disease. *Neurology* 1984;34:939–944.
11. Folstein MF, Folstein SE, McHugh PR. "Mini mental state." A practical method for grading the cognitive state of patients for the clinician. *J Psychiatr Res* 1975;12:189–198.
12. Roth ET, Mountjoy CQ, Huppert FA, Hendrie H, Verma S, Goddard A. CAMDEX. A standardised instrument for the diagnosis of mental disorder in the elderly with special reference to the early detection of dementia. *Br J Psychol* 1986;149:698–709.
13. Chang LT. A method for attenuation correction in radionuclide computed tomography. *IEEE Trans Nucl Sci* 1978;25:638–639.
14. Minoshima S, Berger KL, Lee KS, Mintun MA. An automated method for rotational correction and centering of three-dimensional functional brain images. *J Nucl Med* 1992;33:1579–1585.
15. Minoshima S, Koeppe RA, Mintun MA, et al. Automated detection of the intercommissural line for stereotactic localization of functional brain images. *J Nucl Med* 1993;34:322–329.
16. Minoshima S, Koeppe RA, Frey KA, Ishihara M, Kuhl DE. Stereotactic PET atlas of the human brain: aid for visual interpretation of functional brain images. *J Nucl Med* 1994;35:949–954.
17. Minoshima S, Koeppe RA, Frey KA, Kuhl DE. Anatomic standardization: linear scaling and nonlinear warping of functional brain images. *J Nucl Med* 1994;35:1528–1537.
18. Talairach J, Tournoux P. *Co-planar stereotaxic atlas of the human brain*. New York: Thieme, 1988.
19. Akiyama H, Harrop R, McGeer PL, Peppard R, McGeer EG. Crossed cerebellar diaschisis and uncrossed basal ganglia and thalamic diaschisis in Alzheimer's disease. *Neurology* 1989;39:541–548.
20. Johnson KA, Kijewski MF, Becker A, Garada B, Satlin A, Holman BL. Quantitative brain SPECT in Alzheimer's disease and normal aging. *J Nucl Med* 1993;34:2044–2048.
21. O'Mahony D, Coffey J, Murphy J, et al. The discriminant value of semiquantitative SPECT data in mild Alzheimer's disease. *J Nucl Med* 1994;35:1450–1455.
22. Houston AS, Kemp PM, Macleod MA. A method for assessing the significance of abnormalities in HMPAO brain images. *J Nucl Med* 1994;35:239–244.
23. Dawson MRW, Dobbs A, Hooper HR, McEwan AJB, Triscott J, Cooney J. Artificial neuronal networks that use single-photon emission tomography to identify patients with probable Alzheimer's disease. *Eur J Nucl Med* 1994;21:1303–1311.
24. Lamoureux G, Dupont RM, Ashburn WL, Halpern SE. "CORT-EX": a program for quantitative analysis of SPECT data. *J Nucl Med* 1990;31:1862–1871.
25. Hooper HR, McEwan AJ, Lentle BC, Kothon TL, Hooper PM. Interactive three-dimensional region of interest analysis of HMPAO SPECT brain studies. *J Nucl Med* 1990;31:2046–2051.
26. Hashikawa K, Matsumoto M, Moriwaki H, et al. Three-dimensional display of surface cortical perfusion by SPECT: application in assessing Alzheimer's disease. *J Nucl Med* 1995;36:690–696.
27. Burdette JH, Minoshima S, Vander Borght T, Tran DD, Kuhl DE. Alzheimer's disease: improved visual interpretation of PET images by using three-dimensional stereotaxic surface projections. *Radiology* 1996;198:837–843.
28. Links JM, Devous MD Sr. Detection and comparison of patterns in images. *J Nucl Med* 1994;35:16–17.
29. Mielke R, Grond M, Herholz K, Kessler J, Heiss WD. Age-dependent changes of the metabolic pattern in patients with Alzheimer's disease. In: Maurer K, ed. *Imaging of the brain in psychiatry and related fields*. Berlin: Springer, 1993:171–176.
30. Lantos P. Ageing and dementias. In: Weller R, ed. *Nervous system, muscle and eyes*. Edinburgh: Churchill Livingstone, 1990.
31. O'Brien J, Eagger S, Syed GMS, Sahakian BJ, Levy R. A study of regional cerebral blood flow and cognitive performance in Alzheimer's disease. *J Neurol Neurosurg Psychiatry* 1992;55:1182–1187.
32. Kuhl DE, Phelps ME, Kowell AP, Metter EJ, Selin C, Winter J. Effects of stroke on local cerebral metabolism and perfusion: mapping by emission computed tomography of ^{18}FDG and $^{13}NH_3$. *Ann Neurol* 1980;8:47–60.
33. Kushner M, Tobin M, Alavi A, et al. Cerebellar glucose consumption in normal and pathologic states using fluorine-18-FDG and PET. *J Nucl Med* 1987;28:1667–1670.
34. Talbot PR, Lloyd JL, Snowden JS, Neary D, Testa H. Choice of reference region in the quantification of single-photon emission tomography in primary degenerative dementia. *Eur J Nucl Med* 1994;21:503–508.
35. Saur H-B, Bartenstein P, Oberwittler C, Lerch H, Masur H, Schober O. Comparison of D2 receptor binding (I-123 IBZM) and rCBF (Tc-99m HMPAO) in extrapyramidal disorders. *Nuklearmedizin* 1994;33:184–188.
36. Minoshima S, Frey KA, Foster NL, Kuhl DE. Preserved pontine glucose metabolism in Alzheimer's disease: a reference region for functional brain image (PET) analysis. *J Comput Assist Tomogr* 1995;19:541–547.
37. Mazziotta JC, Frackowiak RSJ, Phelps ME. The use of positron emission tomography in the clinical assessment of dementia. *Semin Nucl Med* 1992;22:233–246.
38. Mielke R, Herholz K, Grond M, Kessler J, Heiss WD. Differences of regional cerebral glucose metabolism between presenile and senile dementia of Alzheimer type. *Neurobiol Aging* 1992;13:93–98.